Characterisation of factors contributing to the performance of nonwoven fibrous matrices as substrates for adenovirus vectored vaccine stabilisation

Authors

Pawan Dulal[1]*, Adam A Walters[1], Nicholas Hawkins[2], Tim DW Claridge[3], Katarzyna Kowal[4], Steven Neill[4], Stephen J Russell[4], Adam Ritchie, Rebecca Ashfield[1], Adrian VS Hill[1], Alexander D Douglas[1]*

*Corresponding authors: pawan.dulal@ndm.ox.ac.uk; sandy.douglas@ndm.ox.ac.uk

Affiliations

1. Jenner Institute, University of Oxford, Wellcome Trust Centre for Human Genetics, Roosevelt Drive, Oxford, OX3 7BN, United Kingdom

2. Oxford Silk Group, ABRG, Department of Zoology, University of Oxford, OX2 3RE, United Kingdom

3. Department of Chemistry, University of Oxford, Chemistry Research Laboratory, Mansfield Road, Oxford, OX1 3TA, United Kingdom

4. Nonwovens Innovation & Research Institute Ltd, 169 Meanwood Road, Leeds, LS7 1SR, UK

Author contributions

Conceptualization, funding acquisition, project administration, supervision: PD, AAW, ADD, SJR, AR, RA, AVSH; Investigation: PD, NH, TDWC, KK; Writing- original: PD, ADD; Writing- review and editing: All

Acknowledgments

Funding

Competing interests

AVSH and ADD are named inventors on patents relating to adenovirus-vectored vaccines.

Abstract

The global network of fridges and freezers known as the "cold chain" can account for a significant proportion of the total cost of vaccination and is susceptible to failure. Cost-efficient techniques to enhance stability of vaccines could prevent such losses and improve vaccination coverage, particularly in low income countries. We have previously reported a novel, potentially less expensive thermostabilisation approach using a combination of simple sugars and glass micro-fibrous matrix, achieving an excellent recovery of vaccines after storage at supraphysiological temperatures. This matrix is, however, prone to fragmentation and currently not suitable for clinical translation.

Here, we report an investigation of alternative, potentially GMP compatible, fibrous matrices. A number of commercially-available matrices permitted good protein recovery, quality of sugar glass and moisture content of the dried product but did not achieve the thermostabilisation performance of the original glass fibre matrix. We therefore further investigated physical and chemical characteristics of the glass fibre matrix and its components. Our investigation shows that the polyvinyl alcohol present in the glass fibre matrix assists vaccine stability. This finding enabled us to develop a custom-produced matrix with encouraging performance, as an initial step towards a biocompatible matrix for clinical translation. We discuss the path to transfer of the technology into clinical use, including potential obstacles.

Introduction

Vaccine immunogens are composed of complex biological macromolecules. Good immunogenicity requires stability of these molecules throughout the lifespan of a product, from production and formulation, through transportation and storage to delivery to the recipient. Extrinsic factors such as light, pH, agitation and oxidants combine with temperature fluctuations to challenge product stability. Therefore, most vaccines need to be continuously stored in fridges or freezers. Maintaining the cold chain and associated logistics in vaccination campaigns can contribute up to 45% of the total cost of vaccination [1]. On the other hand, damage as a result of cold chain breakages costs several million dollars annually [2]. These issues affect not only low income countries, where the cold chain is regarded as being least reliable, but also developed countries [3] [4] [5]. The vaccines responsible for eradication of smallpox and rinderpest (the only two diseases eradicated by immunisation) were both thermostable, a factor believed to contribute to their success [6]. Development of technologies to enhance vaccine thermostability has therefore been a major focus of research effort [7].

Viral vectored vaccines, in particular adenoviruses, are versatile platforms for development of novel vaccines against malaria [8] [9], HIV -AIDS [10] [11], tuberculosis [12] and influenza [13] [14]. They have provided one of the leading approaches to control of the recent Ebola epidemics, and the speed of producing new vaccines using a generic manufacturing process makes them attractive for emergency response to other outbreak pathogens [15,16]. Successful thermostabilisation of adenovirus vectored vaccines could thus be valuable for products targeting a wide range of diseases.

There have been a number of efforts to enhance stability of adenovirus-based vaccines in liquid formulation [17-19]. Other groups have reported improvement in stability by drying vaccines using lyophilisation [20,21], spray drying [22-24], and nano-patch technology [25]. We have previously reported that drying a formulation of adenovirus in glass forming sugars upon a fibrous matrix such as paper or a wetlaid nonwoven fabric permitted full recovery of viable and immunogenic virus, even after six months at 45°C [26-28]. We refer to this method as sugar-matrix thermostabilisation (SMT). As well as

79   thermostabilisation performance, advantages of SMT include a relatively short process duration (in

80   some cases as little as 18 hours) and avoidance of the stress of extreme in-process temperature

81   exposure involved in lyophilisation and spray drying.

82   Our previous published SMT work used a glass fibre matrix and a polypropylene matrix; we reported

83   that the glass fibre matrix achieved better stability than the polypropylene matrix [26]. Glass fibre

84   matrix is however prone to shedding of non-biocompatible fibres, and so not suitable for clinical

85   translation. Here, we present results from an effort to characterise the factors contributing to the

86   performance of glass fibre matrix and to test alternative matrices more suitable for clinical use.

87

Methods

Viruses and infectivity titration

Simian adeno virus vectors ChAd63-METRAP and ChAdOx2-RabGP were prepared, purified and tested for quality by the Jenner Institute Viral Vector Core Facility, as previously described [28,29]. Viruses were dialysed against either a previously used storage buffer (10mM Tris, 7.5 % w/v sucrose, pH 7.8) or unbuffered 0.5M trehalose and sucrose and stored at -80°C as stock. Typical preparations were supplied and stored at a titre of c. 1×10^{12} virus particles (VP) per mL, corresponding to c. 1×10^{10} infectious units (IU) per mL and hence a particle: infectivity ratio of c. 100.

For infectivity titration, duplicate fivefold serial dilutions were prepared in complete DMEM (10% FCS, 100 U penicillin, 0.1 mg streptomycin/ml, 4 mM L-glutamine) and used to infect 80-100 % confluent HEK293-TRex cells (ThermoFisher) grown in 96-well plates (BD Purecoat Amine, BD Biosciences, Europe). Infected cells were immunostained and imaged as previously described [30]. Wells containing 20-200 spots were used to back-calculate recovered infectious units.

Drying, thermochallenge and reconstitution

Stock vaccines were thawed and diluted into unbuffered 0.5M trehalose – sucrose solution. Dilution factors, final viral titres, and the trehalose: sucrose ratio varied between experiments, as stated in figure legends.

Fibrous matrix was cut into 100 mm² pieces, loaded with vaccine formulation and transferred to a glove box (Coy Laboratory Products). An activated silica bed within the chamber and circulation of air through desiccation capsules containing anhydrous calcium sulphate (Drierite™, W.A. Hammond Drierite Co.), regulated by a humidity controller (Series 5000, Electro-tech Systems), was used to maintain relative humidity beneath 5%. A portable datalogger (AET-175, ATP instruments) was used for recording changes in relative humidity and temperature during the desiccation process. The temperature inside the enclosed glove box remained between 22°C and 25°C for all experiments.

113 Samples were transferred into 2 mL glass vials, stoppered and crimp sealed under dry conditions

114 within the glove box prior to further use. Samples undergoing thermochallenge i.e. storage at

115 elevated temperature (typically 45°C for one or four weeks) were stored within secondary packaging

116 (moisture barrier bags).

117 For experiments involving reconstitution of dried samples, this was performed by addition of

118 phosphate buffered saline (Sigma), followed by brief vortexing of the vial (1±0.5 seconds, three

119 times). Virus infectivity after reconstitution was assayed as described above. Recovery of infectious

120 virus was quantified by comparison to a sample of the starting material, included on the same assay

121 plate. Between the set-up of an experiment and the assay of recovered infectivity, such comparator

122 material was stored at -80°C in aqueous buffer (under which conditions loss of infectivity is known to

123 be negligible).

124 Recovery was calculated in terms of $\log_{10}$-fold loss in the total infectious virus content of the matrix

125 i.e. $\log_{10}$-fold loss = $\log_{10}$(infectious units dried on matrix based on -80 stored sample) −

126 $\log_{10}$(infectious units recovered from matrix). Unlike viral titres (infectious units / mL), this

127 parameter is independent of the volumes in which sample was dried or reconstituted. 0.3 $\log_{10}$-fold

128 loss thus implies c. 50% recovery, 0.5 $\log_{10}$-fold loss implies c. 30% recovery, and 1 $\log10$-fold loss

129 implies 10% recovery.

130

131 ## Karl Fischer moisture analysis

132 Residual moisture content in single matrix post-desiccation was determined with a Karl Fischer

133 moisture analyser equipped with coulometer (Metrohm), and Hydranal-Coulomat titration solution

134 (Honeywell, Fluka) in accordance with the manufacturers' recommendations. A standard was used

135 to calibrate the instrument performance (lactose standard 5%, MerckMillipore). Residual moisture

136 content was expressed as the mass extracted per 50 µL of formulation loaded into each matrix.

Measurement of subvisible particles

137

138 100 mm^2 pieces of glass fibre (S14) were cut, autoclaved at (121 ^{o}C, 15 minutes) and loaded with 50

139 μL of sugar solution prior to drying in the glove box, vialling and reconstitution as described above.

140 Reconstituted solution from 10 vials was aspirated using a syringe with a conventional 20G needle

141 (BD Biosciences), to produce a single pooled unfiltered sample. Reconstituted solution from a

142 further 10 vials was aspirated using a 5-micron filter needle (BD Biosciences), to produce a single

143 pooled filtered sample. Both pools were diluted to a final volume of 25 mL and tested for sub-visible

144 particles by light microscopy according to Ph.Eur (2.9.19) / USP <788> by a commercial testing

145 laboratory (Reading Scientific Services Limited).

146

Scanning electron microscopy

147

148 Untreated matrices (i.e. without sputter coating) were loaded onto aluminium mounts using carbon

149 conductive tabs and imaged using a Zeiss-Evo LS15 variable pressure scanning electron microscope

150 (SEM) equipped with variable pressure secondary electron detector (Carl Zeiss Ltd). Imaging was

151 performed at a chamber pressure of 50 Pa air and accelerating voltage of 15 kV. Further analyses of

152 images such as measurement of fibre diameter were made using Image J software. At least 40

153 measurements per matrix were performed, using images taken at varying magnification.

154

Differential scanning calorimetry

155

156 The glass transition temperature (T_g) of sugar glass in matrices was measured immediately after

157 drying had completed using Differential Scanning Calorimetry (DSC). The melting point of the binder

158 in untreated glass fibre (S14) was measured using DSC (Q2000, TA instruments). The instrument was

159 purged with dry nitrogen (50 mg/mL) continuously during sample measurement. Calibration was

160 performed prior to measurements using a certified reference material (Indium) for temperature and

161 heat flow accuracy.

162   Multiple 6-millimetre diameter discs were cut out of a matrix dried with 0.5M trehalose: sucrose

163   (50:50). Discs were weighed and, for each matrix type in turn, a total mass of 5-15 milligrams was

164   loaded into Aluminium DSC pans (TA Instruments) and hermetically sealed. Samples were subjected

165   to a temperature ramp from -20 °C to 180 °C at a heating rate of 10 °C per minute. Measurements

166   on all samples were performed in duplicates. Thermograms relating heat flow (W/g) to temperature

167   (°C) were analysed using Trios software (TA Instruments) for identification of the glass transition (Tg)

168   onset temperature.

169   For the measurement of enthalpic recovery, which manifests as an endothermic peak at the glass

170   transition, modulated DSC (temperature modulation ±0.50°C every 60 seconds and ramp rate

171   3°C/min from -20°C to 100°C) was employed. The enthalpic recovery was estimated by linear peak

172   integration in the thermograms plotted between nonreverse heat flow (W/g) and temperature (°C)

173   using Universal Analysis software (TA Instruments).

174

Protein recovery

176   A 10mg/mL solution of lysozyme (Sigma-Aldrich) was made in 0.5M trehalose sucrose. 25 μL was

177   loaded into each matrix in triplicates. Protein was reconstituted from the matrices after desiccation

178   overnight and recovery was quantified using EnzChek Lysozyme Assay Kit (ThermoFisher Scientific).

179   Fluorescence measurements were performed in triplicates for each sample and protein recovery

180   calculated by interpolation on a standard curve, using GraphPad Prism.

181

Thermogravimetric analysis

183   Degradation temperatures of matrix constituents were measured by thermogravimetric analysis

184   using a TGA Q500 (TA instruments). Samples loaded into a tared platinum pan just prior to

185   measurement were subjected to a temperature ramp at 5°C per minute from ambient to 550°C in a

186   flowing nitrogen atmosphere (100ml/min). The gas was switched to air at 550°C (100 ml/min) and

187 heat was continued at the rate of 5°C/min to 730°C. Data was analysed using Universal Analysis

188 software (TA Instruments).

189

Polyvinyl alcohol (PVA) extraction and Fourier transform infrared spectroscopy

191 A 500 mm X 27 mm piece of glass fibre (S14) was dissolved in 100 mL of ultrapure water by stirring

192 and heating at 90 °C for 48 hours. The suspension was filtered through a 0.2 μm filter and the filtrate

193 was freeze dried (Virtis AdVantage 2.0, SP Scientific) to a white amorphous material. This residue

194 was subjected to single reflection attenuated total reflection (MIRAacle ™, Pike Technologies)

195 Fourier transform infrared spectroscopy ATR-FTIR (Tensor 37, Bruker) equipped with nitrogen-

196 cooled mercury cadmium telluride detector.

197 To obtain a spectrum of the sample, an average of 64 interferograms was collected at a resolution of

198 4 cm^{-1} in the wavelength range from 4000 cm^{-1} to 750 cm^{-1} and blank subtracted.

199 Spectra were analysed using OPUS 6.5 software (Bruker) and compared with RMIT University's

200 spectral library of organic compounds generated using Spectrum 10 software (Perkin Elmer).

201 Fingerprint spectra shown in Figure 4D were prepared using GraphPad Prism.

202

Dynamic light scattering (DLS)

204 The molecular weight of the PVA binder present on the glass fibre matrix (S14) was estimated by

205 DLS. PVA was extracted and freeze-dried as described above. Solutions of this extracted sample and

206 standards of known polymer size were prepared in water to the concentration of approximately 1.3

207 mg/mL and passed through 0.22 μm and 300 kDa molecular weight cut-off filters. The sample was

208 then concentrated approximately five-fold from 4mL to 0.75 mL using a 3KDa MWCO filter (Vivaspin,

209 GE). Zetasizer Nano ZS and DTS software (Malvern Instruments) was used for measurement of

210 hydrodynamic diameter based on size distribution by volume. Independent duplicate preparations

211 of all standards and samples were tested. GraphPad Prism was used to generate a standard curve

212   plotted between measured hydrodynamic diameter and known average molecular weight (KDa) to

213   interpolate size of the PVA in the extract.

Nuclear magnetic resonance (NMR) spectroscopy

215   The degree of hydrolysis of the PVA binder present on the glass fibre matrix (S14) was estimated by

216   ^{1}H NMR measurement as the intensity of the peak attributable to the acetyl group present in non-

217   hydrolysed PVA. A 5 mg/mL aqueous solution of PVA extracted from the glass fibre sample (S14) was

218   prepared in deuterium oxide. Reference spectra for PVA with varying degrees of hydrolysis were

219   obtained by mixing >99% hydrolysed PVA and 80% hydrolysed PVA in appropriate proportions to

220   produce standards containing c. 0%, 2%, 5%, 10% and 20% acetyl groups, again at 5 mg/mL in

221   deuterium oxide. An AVIII 700 instrument (Bruker Biospin) was used to generate ^{1}H 1D spectra

222   (employing a quantitative 1D NOESY (Nuclear Overhauser Effect Spectroscopy) presaturation

223   sequence with recovery delay d_1 =30s) and 2D ^{1}H-^{13}C HSQC (heteronuclear single quantum

224   coherence spectroscopy) plots.

Application of PVA to matrices

226   Aqueous solutions of each type of PVA to be investigated were prepared at 10 mg/mL. Matrices

227   were cut into approximately 100 mm^2 pieces and loaded with until the matrices were saturated by

228   the solution and air-dried overnight. The polyamide matrix (33100L) required surface modification

229   by washing in 100% ethanol for 20 minutes and air drying before PVA could be loaded. Following

230   PVA application, vaccines were dried on the matrices and thermostability assessed as described

231   above.

Study of physical characteristics of matrices

233   The physical characteristics of matrices were studied using NWSPs (Nonwoven Standard Procedures)

234   prescribed by the EDANA, the international trade association for the nonwoven industry.

235   Areal density was measured as ratio of mass in grams and area in square metres according to EDANA

236   NWSP 130.1R0 (15).

237   Matrix thickness was measured at an applied pressure of 0.5 kPa according to EDANA NWSP

238   120.1.R0 (15) using a thickness tester (ProGage, Thwing-Albert Instrument Company).

239   Fibre length was measured based on 60 individual fibres extracted from the matrix using a Leica MD

240   G41 optical microscope in transmission mode and Image J software.

241   Minimum mean and maximum pore size were obtained using a POROLUX 100 Automated Capillary

242   Flow Porometer using Galpore liquid of surface tension 15.6 mN·m$_{-1}$. A total of five measurements

243   were taken per sample. Porosity (ε) of the GE S-14 was determined by the equation ε= (1−Ø) X 100 %

244   where Ø is the volume fraction measured as a ratio of bulk matrix density to bulk fibre density.

245   The surface tension of aqueous sugar solution on the matrix was measured on a Kruss K100

246   tensiometer using the Wilhelmy plate method in which the force exerted on a suspended plate

247   when it touches the surface of a liquid is related to the surface tension and the contact angle

248   according to the equation $\sigma = \dfrac{F}{L.\ cos\theta}$ where σ= surface tension of the liquid, F=measured force,

249   L=wetted length, and Θ=contact angle.

250   Wettability was evaluated using the Washburn method, again on a Kruss K100 tensiometer. The rate

251   of mass uptake when the porous substrate (matrix) comes in to contact with a liquid was used to

252   determine the capillary constant of the substrate by applying the Washburn equation $\dfrac{m^2}{t} = \dfrac{c.\ \rho^2 cos\theta}{\eta}$,

253   where m=mass, t=flow time, c=capillary constant of the nonwoven, ρ=density of the liquid, σ=

254   surface tension of the liquid, Θ=contact angle, η=viscosity of the liquid. The capillary constant of the

255   matrix was determined using n-hexane which has a contact angle of 0°.

Development of Nonwoven Fabrics for Vaccine Thermostabilisation

256   A glass fibre matrix (Figure 5B) was custom made by a wet-lay process using commercially available

258   glass fibre and polyvinyl alcohol aiming for similar porosity, thickness, areal density and wetting

259   behaviour as the glass fibre sample (S14). A matrix of glass fibre type 475 with diameter 4 μm (Johns

260   Manville) was prepared and 1 g/L PVA solution (>99% hydrolysed, Mw 146000-186000 kDa, Sigma)

261   was applied to each side using a spray gun before drying at 110°C for 15 minutes.

262

Results

Glass fibre matrix achieves good stability but is not suitable for clinical development

In our previously published work, we had used low vaccine doses (1.1×10^{10} viral particles per matrix, as compared to a typical human dose of 5×10^{10} viral particles), applied to the glass fibre matrix 'Standard 14' (S14, GE Healthcare, Figure 1A) [26]. We speculate that the fibrous matrix provides a high surface area, favouring relatively rapid drying of the product despite the gentle conditions used (18-24 hours at 20-23 °C and atmospheric pressure). The process results in films of vitreous 'sugar glass' embedded in the matrix (Figure 1B). As previously reported, this 'base-case' process achieves a sugar glass transition temperature (T_g) after drying of 47-55°C, with moisture content 3-5% of total solute dry weight [26].

We have now dried full human doses (5×10^{10} virus particles, approximately 5×10^8 infectious units [IU]) of a simian adenovirus vectored rabies vaccine (ChAdOx2 RabG) upon 1 cm^2 of the matrix, with <0.1 log$_{10}$-fold loss in-process (i.e. during desiccation) and approximately 0.3 log$_{10}$-fold loss after thermochallenge at 30°C for a month (Figure 1C) [28]. For explanation of the log$_{10}$-fold loss metric, please see Methods.

Despite the good thermostabilisation performance of the glass fibre matrix, concerns were raised regarding the brittleness of glass fibre would result in shedding of fibres during the process of vaccine reconstitution. Indeed, macroscopic damage to the matrix was sometimes apparent at the point of reconstitution. We therefore sought to quantify subvisible particles (0.1-100 micron) in the reconstituted vaccine. Application of a pharmacopoeial light microscopy method revealed numerous glass fibres (Figure 1D). Although passing the reconstituted solution through a 5 µm filter needle removed virtually all detectable glass particles, reducing the particulate burden within pharmacopoeial limits, such a method is unsuitable for clinical development, with the possible exception of very early-phase studies [31].

Selection of commercially-available matrices for evaluation

In our previously published work, we reported that the S14 matrix achieved better vaccine thermostability than an alternative commercially-available polypropylene-based matrix (HDC®II J200, Pall Corporation). We therefore sought to identify alternative commercially-available matrices which might offer thermostability equivalent to or better than that achieved with S14, but without the problem of shedding of non-biocompatible fibres. A set of seven matrices were selected based on manufacturers' product specifications claiming low fibre shedding, low chemical leaching and compatibility with sterilisation either by dry heat, steam or gamma-radiation sterilisation (Table 1). Henceforth matrices are referred to, for clarity of identification, in terms of their fibre material and the manufacturer's product name.

We initially screened all matrices for suitable loading capacity (>20 μL of deionised water/cm^2). Matrices which did not absorb 20 μL/cm^2 (without visible remaining beads of water within two seconds) were re-tested after treatment with 2% polysorbate 20 solution. Matrices which did not absorb 20 μL/cm^2 after detergent treatment were not studied further. We proceeded to further study of the remaining five matrices along with the two previously tested matrices (glass fibre S14 and polypropylene J200).

The architecture of the selected matrices was characterised by scanning electron microscopy (Figure 2). Fibre diameters estimated for each matrix type using Image J analysis are presented in table 1.

Fibres in the polypropylene (J200) matrix (Fig 2A) and glass fibre (conjugate pad) matrix (Fig 2F) shared the straight, rod-like fibre morphology seen in the original glass fibre (S14) matrix (Fig 1A-B) but had larger fibre diameters of 10 – 20 μm (as compared to 4 μm in the S14 glass fibre sample). The remaining four matrices (Fig 2B-E) exhibited a greater degree of curl along their length. A film, potentially a binder, was apparent on the glass fibre matrix (conjugate pad) (Fig 2F). Matrices loaded with 0.5 M sugar solution and dried at room temperature for 24 hours also showed differences in

312   the distribution of the sugar glass intercalated between the fibres**Error! Reference source not**

313   **found.**(Figure 2). Distinct films of sugar glass between the fibres were visible on the two glass fibre

314   matrices, but not in the polyamide (33100L), polyester (leukosorb) or polypropylene (J200) matrices.

315   The sugar loaded polyester (23100) matrix and cellulose (31 ET CHR) matrices showed a glazing

316   effect on the fibres, with discrete sugar glass films being apparent.

317

Thermostability of adenovirus vaccine formulated in commercially-available matrices

Adenovirus vaccine vectors were formulated in 0.5M TS and dried on the five selected 'new' matrices, with glass fibre (S14) and polypropylene (J200) matrices as comparators of known performance. Dried matrices were thermochallenged for a week at 45°C prior to reconstitution and infectivity titration. Marked thermostabilisation performance differences between the matrices were apparent (Table 1).

As previously observed, the glass-fibre matrix (S14) showed minimal (less than 0.3 $\log_{10}$-fold) loss of infectivity compared to the -80 ^{o}C stored positive control. None of the alternative matrices matched this level of performance: the next-best-performing matrices were polyamide (33100L) and glass fibre (conjugate pad), with infectivity loss of 0.9 $\log_{10}$-fold in each. The cellulose-based matrix (GE) performed most poorly.

Relationships between matrix type, thermostabilisation performance and physical characteristics of sugar glass

In order to understand the highly variable thermostabilisation performance of the matrices, we investigated whether performance could be correlated with the physical properties of the matrices or the sugar glass formed.

Standard sugar formulation (0.5M trehalose sucrose) was loaded into each matrix and dried at room temperature and < 5% relative humidity. Dried samples were then subjected to modulated differential scanning calorimetry (DSC) to measure glass transition temperature (Tg) onset temperature and enthalpic recovery of the sugar glass formed on the matrices. The glass transition temperature (T_g) indicates the temperature at which a low mobility sugar glass changes to a highly mobile rubbery state and is known to be related to product stability in dry formulations [32]. Enthalpic recovery is a measure of energy dissipated as a glass progresses through equilibrium and can reflect molecular rearrangement during storage or physical ageing [33].

344   The T_g was similar for all matrices, observed over a narrow range between 52°C and 56°C, and did

345   not correlate with thermostability (Figure 3A). A possible correlation was observed between

346   thermostabilisation performance and high enthalpic recovery (Figure 3B, r^2=-0.70, p=0.02), as seen

347   with glass fibre matrices conjugate pad and S14 followed by polypropylene (J200) based matrix.

348   There was substantial variation in the residual moisture content of products dried under the same

349   conditions on different matrices (Figure 3C), with lowest residual moisture in the best performing

350   matrix, S14. Recovery of a model protein (lysozyme) after desiccation and reconstitution did not

351   predict thermostabilisation performance (Figure 3D).

352

353   ## Characterisation of S14 glass fibre matrix

354   Given our inability to identify a commercially-available matrix suitable for clinical application, we

355   turned our attention to detailed characterisation of the best-performing S14 matrix, with a view to

356   future production of a similar matrix from biocompatible materials.

357   We initially performed a more extensive characterisation of the physical properties of the matrix,

358   with results as shown in Table 2.

359   Use of chemical binders is common in the production of nonwoven fabrics such as S14 to provide

360   strength and desirable surface properties. In view of the possibility that a binder might be

361   contributing to S14's thermostabilisation performance, we investigated whether such a binder could

362   be identified in the matrix.

363   Scanning electron microscopy demonstrated film-like material which could represent binder

364   covering fires in some sections of the S14 sample (Figure 4A). Differential scanning calorimetry and

365   thermogravimetric analysis (Figures 4B-C) demonstrated the presence of a material with a melting

366   point of 220°C and a degradation temperature at 260°C.

367   For further characterisation, the binder was extracted in liquid and freeze dried. Fourier transform

368   infrared (FTIR) spectroscopy of the extract provided a fingerprint spectrum, which matched closely

369   with the expected spectrum of polyvinyl alcohol (PVA) (Figure 4D) [34,35].

370   The solubility and other properties of PVA vary widely according to molecular weight (MW) and

371   degree of hydrolysis, and so we sought to further characterise the presumed PVA extracted from

372   S14. We used dynamic light scattering (DLS) to compare the hydrodynamic radius of the PVA extract

373   to those of PVA samples of known MW. The results were consistent with a MW in the range of 35

374   kDa (Figure 4E).

375   We then used 1H NMR to estimate the degree of hydrolysis of the polymer. The 1H NMR spectrum

376   obtained (Figure 4F) was consistent with PVA, with a 2:1 ratio of the areas under the peaks at ~1.6

377   ppm and 3.9 ppm (corresponding to hydrogens in the CH_2 and CH environments respectively).

378   Results obtained using a range of standards of varying percentage hydrolysis showed a clear

379   relationship of the size of a peak at 2.05 ppm to the acetyl group content (the presence of which, in

380   a sample of PVA, indicates incomplete hydrolysis). The spectra of the completely hydrolysed

381   standard and the S14 extract were similar, with only a trace of a peak in this area, and so we

382   concluded that the PVA extracted from S14 is likely to be completely hydrolysed.

383

PVA enhances adenovirus stabilisation by SMT

385   Having identified PVA in the best-performing matrix, S14, we investigated whether the PVA may

386   function not only as a binder but might actually contribute to vaccine thermostabilisation.

387   We reasoned that treatment with PVA might enhance the thermostabilisation performance of

388   relatively poorly-thermostabilising matrices. We observed that application of PVA extracted from

389   glass fibre (S14) significantly improved thermostabilisation performance of two of the three tested

390   matrices, as assessed by infectious virus recovery after a four week 45 °C thermochallenge. Recovery

391   from the polyester matrix (Leukosorb) was enhanced by 1.3 log_{10}-fold, while enhancement from the

392   cellulose matrix (ET CHR) was enhanced by 2 $\log_{10}$-fold (Figure 5A). Addition of PVA to a glass fibre

393   matrix (Pall's conjugate pad) was not beneficial. This matrix already contains a binder (Fig 2F),

394   possibly PVA.

395   We proceeded to test whether the degree of hydrolysis of PVA had any impact on vaccine

396   thermostability at 45°C for an extended period of 28 days. We tested polyester (Leukosorb),

397   polyamide (33100L) and a custom-made glass fibre-based matrix after treatment with PVA extracted

398   from S14 and two other commercially sourced polymers (Sigma) which were similar in size but

399   differed in degree of hydrolysis (30-70 KDa / 87-90% hydrolysed, and 31-50 KDa/ >99% hydrolysed).

400   We again observed substantial improvements in thermostabilisation performance, exceeding a 1

401    $\log_{10}$-fold increase in infectious virus recovery after thermochallenge, when PVA was applied to

402   matrices which did not contain PVA at baseline (polyamide and polyester) (Figure 5B). The greatest

403   enhancement was seen with the S14 extract, followed by the fully hydrolysed PVA, with the least

404   enhancement seen with the incompletely hydrolysed PVA (Figure 5B).

405

Towards development of custom nonwoven fabrics for vaccine thermostabilisation

408   Having characterised the geometry and composition of S14, and the contribution of PVA to its

409   thermostabilisation performance, we proceeded to develop a bespoke matrix 'in-house'. Although

410   our ultimate aim is to produce biocompatible matrices, we sought as an initial step to test whether

411   the understanding we had gained would enable us to produce an 'in-house' wet-laid glass fibre

412   matrix which could replicate S14's thermostabilisation performance. The new matrix had structural

413   properties similar to those of S14 (area density 50.6±1.5 g.m^{-2}, thickness 0.56±0.02 mm, mean flow

414   pores 25±2.3 μm, absorption capacity 11.1±0.3 g/g, composed of borosilicate glass fibres with

415   diameter 3.6±1.8 and length 1.3±0.6 mm; see table 2 for data relating to S14), and a similar

416   appearance (Figure 5C). Although thermostabilisation performance of the custom-made matrix did

417   not exactly match that of S14 (Figure 5D), it was closer than had previously been achieved with any

418   of the other tested matrices (Fig 5B). As expected, further modification of the matrix with additional

419   PVA had no effect.

Discussion

421   The starting point for the present study was the observation, in our previous work, that the non-

422   biocompatible glass-based S14 matrix out-performed a polypropylene matrix [26]. This posed the

423   question of which properties of the matrix could be relevant for SMT performance, and whether a

424   more suitable matrix than S14 could be identified for clinical translation.

425   Our initial attempts to find a suitable commercially available matrix yielded disappointing results.

426   Adenovirus stability on the tested matrices was poor (table 1). Multiple variables differed between

427   each matrix, and we were therefore unable to perform experiments to clearly isolate the effect of a

428   single variable. There was not a clear relationship between characteristics of the matrices and their

429   stabilisation performance (Figures 2 and 3), with the possible exception of high enthalpic recovery of

430   sugar glass (which is not a parameter which can readily be 'designed in' to a new matrix).

431   Our ability to use analysis of commercially available matrices to draw conclusions to guide design of

432   new biocompatible matrices was thus limited. We therefore changed our strategy, seeking to

433   characterise S14 in detail and produce similar matrices 'in-house', allowing us to identify features of

434   S14 contributing to its stabilising performance.

435   Most significantly we found that PVA, present on the S14 matrix as a binder, appears to contribute

436   to the stability of adenovirus (Figures 4 and 5). It was shown that fully hydrolysed PVA, similar to

437   that we extracted from S14, was most beneficial in thermostabilisation (Figure 5). Polyvinyl alcohol is

438   potentially suitable for use as an excipient in vaccine formulations: it is 'generally regarded as safe'

439   (GRAS) and is also a FDA approved inactive ingredient for parenteral use [36]. PVA has previously been

440   explored as an excipient in a number of studies of bio-macromolecular stability. It has been found to

441   be beneficial in some formulations of proteins, including insulin [37], but benefit has not been seen

442   consistently in other studies [38] [39] [40]. PVA may contribute to protein stability by hydrogen bonding of

443   hydroxyl groups in PVA to the proteins. In dried protein formulations, PVA has also been shown to

444   prevent deamidation more potently than another widely used polymeric excipient, polyvinyl

445   pyrrolidone [41].

446   We now intend to develop the SMT method towards clinical application. There are two principal

447   obstacles to this goal: robust and GMP compliant execution of the process, and the availability of a

448   suitable matrix for GMP production. Robustness and GMP compliance of the process are clearly

449   interlinked. We believe several of the challenges of GMP execution of the SMT process can be

450   addressed by execution of drying within a lyophilizer without freezing or the application of vacuum:

451   existing large-scale GMP lyophilisation facilities could provide the necessary controlled temperature,

452   low humidity, aseptic environment. With respect to robustness, we have found in recent work that

453   the stability achieved by the process can be highly sensitive to deviations from the intended

454   conditions and, more troublingly, some unexplained inconsistency in performance can occur: work is

455   ongoing to address these issues. With respect to the matrix, GMP execution is likely to require

456   development of a new non-woven. In addition to replicating the stabilising performance of S14, such

457   a matrix needs to be biocompatible, to have good mechanical integrity (in particular, without

458   shedding fibres into the reconstituted product), and to be produced in line with the quality

459   requirements for a GMP raw material. We are now using the data provided by the present study in

460   order to develop such a matrix, mimicking the physical properties of S14 and making using of the

461   beneficial effect of PVA, but without the problematic use of glass.

462   [END]

463

Figure Legends

Figure 1: SMT on S14 results in thermostable vaccine embedded in sugar glass,

Panels A and B show scanning electron micrographs of S14, respectively before and after loading and drying sugar formulation. In Panel A, the arrangement of fibres in S14 is apparent (200X magnification, 100 μm scale bar). In panel B, sugar glass films are visible between fibres (main panel at 200X magnification with 100μm scale bar, inset at 1000X magnification with 20μm scale bar).

Panel C shows recovery of vaccine from matrix loaded with a human dose of adenovirus, both immediately post-drying and after thermochallenge at 30 $^{\circ}$C for one month. Results plotted illustrate total virus recovery from each replicate matrix (n=4 for -80 $^{\circ}$C comparator, n=2 for post-drying, n=3 for post-thermochallenge), with lines indicating the mean of the replicates. Numbers above each result show $\log_{10}$-fold loss from the -80 $^{\circ}$C control.

Panel D shows a representative light microscopy image of fibres shed from S14 after vaccine reconstitution (scale bar 200 μm).

478   Figure 2: Physical appearance of fibres and sugar glass formed in matrices

479   Scanning electron microscopy images of six different matrices at 1000X magnification. Within each

480   panel, the left-hand image shows empty matrices and the right-hand image shows sugar-loaded

481   fibres. Scale bar shows 20 µm in each image.

482

483 ## Figure 3: Physical properties of sugar glass have differential impact on vaccine
484 ## thermostability

485 Each panel relates the thermostabilisation performance of the various matrices (after one-week

486 thermochallenge at 45 °C, Y-axis, data shown in Table 1) to a potentially explanatory variable on the

487 X-axis: glass transition temperature (Panel A); enthalpic recovery (Panel B); moisture content (Panel

488 C); and protein recovery (Panel D). Results of Pearson correlation analysis are shown within each

489 panel. DSC measurements (Panels A and B) were made in singlicate, Karl-Fischer measurements

490 (Panel C) were made in duplicate, and protein recovery measurements (Panel D) were made in

491 triplicate. For panels C and D, points represent the mean measurement.

492

493 ## Figure 4: Chemical properties of glass fibre matrix

494 Panel A shows a scanning electron microscopy image indicating presence of binder in glass fibre

495 (S14), visible as a film in the white-circled area. Scale bar shows 10 μm in each image. Such areas

496 were relatively sparse, compared to the extensive films apparent in sugar-loaded matrices (Figure

497 1B).

498 Panel B shows a differential scanning calorimetry thermogram of glass fibre (S14), representative of

499 duplicate measurements. The graphs show heat flow as a function of temperature during scanning

500 from 40 °C to 250 °C.

501 Panel C displays thermogravimetric analysis of glass fibre (S14), showing a thermal decomposition

502 step. Weight losses (green lines) and the rate of weight loss (i.e. derivative, %/°C) (blue lines) are

503 shown.

504 Panel D shows the sample spectrum obtained from attenuated total reflectance Fourier transform

505 spectroscopy (ATR-FTIR) for the binder recovered from glass fibre (S14) (black), and a reference

506 library spectrum for PVA (grey).

507 Panel E shows estimation of the molecular weight of the binder extracted from glass fibre (S14) by

508 DLS. Points and solid line show a standard curve generated using PVA of known MW. Dashed lines

509 indicate the hydrodynamic radius of the PVA extracted from S14 (11nm) and the inferred MW (36

510 kDa). Points and error bars indicate the mean and range respectively of duplicate DLS

511 measurements.

512 Panel F shows 1H NMR spectra used to estimate the percentage hydrolysis of the binder extracted

513 from glass fibre (S14). The upper spectrum (labelled S14) is that of the extract, with unknown

514 percentage hydrolysis and hence an unknown percentage of monomers bearing acetyl groups. The

515 five spectra below were obtained using standards prepared by proportionately mixing 80% and

516 100% hydrolysed PVA to achieve a range of acetyl group content ranging from <0.1% up to 20% (as

517 per labels to left of panel). The X-axis indicates chemical shift measured in parts per million (ppm)

518 and the Y-axis shows relative intensity.

519   ## Figure 5: PVA improves vaccine thermostability on matrices

520   A PVA-containing extract prepared from S14 was dried onto various fresh matrices, followed by

521   drying of vaccine in trehalose-sucrose buffer onto the treated matrices and untreated comparator

522   matrices. Viable virus recovery was assessed after thermochallenge as indicated for each panel. S14

523   was included as a comparator in each experiment.

524   Panel A shows loss in infectivity titre of vaccine in the absence (open circles) or presence (solid

525   circles) of PVA extracted from glass fibre (S14), as compared to -80°C stored liquid control, after one

526   week at 45 °C. Points indicate individual samples (four replicates per condition).

527   Panel B shows difference in loss in infectivity titre of vaccine loaded in polyester (leukosorb) and

528   polyamide (33100L) matrix modified by deposition of three different types of PVA prior to

529   application and drying of vaccine. Dried samples were subjected to thermochallenge for four weeks

530   at 45 °C. Points indicate individual samples (three replicates per condition).

531   Panel C shows a scanning electron microscope image of the custom-made glass fibre matrix. Scale

532   bar shows 50 μm.

533   Panel D compares loss in infectivity titre of vaccine post-thermochallenge between standard 14 and

534   custom-made glass fibre matrix modified by deposition of two different types of PVA prior to

535   application and drying of vaccine. Dried samples were subjected to thermochallenge for four weeks

536   at 45°C. Points indicate individual samples (three replicates per condition).

537

References

1. Lydon P, Zipursky S, Tevi-Benissan C, Djingarey MH, Gbedonou P, Youssouf BO, Zaffran M. Economic benefits of keeping vaccines at ambient temperature during mass vaccination: the case of meningitis A vaccine in Chad. Bulletin of the World Health Organization 2014; 92(2):86-92.

2. Centers for Disease Control and Prevention. Vaccine Storage and Handling Toolkit. U.S. Department of Health and Human Services (2019). https://www.cdc.gov/vaccines/hcp/admin/storage/toolkit/storage-handling-toolkit.pdf. Accessed November 27, 2019

3. Bell KN, Hogue CJ, Manning C, Kendal AP. Risk factors for improper vaccine storage and handling in private provider offices. Pediatrics 2001;107(6):E100.

4. McColloster PJ. US vaccine refrigeration guidelines: loose links in the cold chain. Hum Vaccin 2011;7(5):574-575.

5. Kristensen D, Chen D, Cummings R. Vaccine stabilization: research, commercialization, and potential impact. Vaccine 2011;29(41):7122-7124.

6. Chen D, Zehrung D. Desirable attributes of vaccines for deployment in low-resource settings. J Pharma Sci 2013;102(1):29-33.

7. Walgate R. Gates Foundation picks 14 grand challenges for global disease research. Bulletin of the World Health Organization 2003;81(12):915 – 916.

8. Hill AVS. Pre-erythrocytic malaria vaccines: towards greater efficacy. Nat Rev Immunol 2006;6(1):21-32.

9. Ewer KJ, Sierra-Davidson K, Salman AM, Illingworth JJ, Draper SJ, Biswas S, Hill AVS. Progress with viral vectored malaria vaccines: A multi-stage approach involving "unnatural immunity". Vaccine 2015;33(52):7444-7451.

562   10. Hanke T, Goonetilleke N, McMichael AJ, Dorrell L. Clinical experience with plasmid DNA- and

563   modified vaccinia virus Ankara-vectored human immunodeficiency virus type 1 clade A

564   vaccine focusing on T-cell induction. J Gen Virol 2007;88(Pt 1):1-12.

565   11. Hanke T. Conserved immunogens in prime-boost strategies for the next-generation HIV-1

566   vaccines. Expert Opin Biol Ther 2014;14(5):601-616.

567   12. Sheehan S, Harris SA, Satti I, Hokey DA, Dheenadhayalan V, Stockdale L, Manjaly Thomas ZR,

568   Minhinnick A, Wilkie M, Vermaak S, Meyer J, O'Shea MK, Pau MG, Versteege I, Douoguih M,

569   Hendriks J, Sadoff J, Landry B, Moss P, McShane H. A Phase I, Open-Label Trial, Evaluating

570   the Safety and Immunogenicity of Candidate Tuberculosis Vaccines AERAS-402 and MVA85A,

571   Administered by Prime-Boost Regime in BCG-Vaccinated Healthy Adults. PLOS ONE

572   2015;10(11):e0141687.

573   13. Rimmelzwaan GF, Sutter G. Candidate influenza vaccines based on recombinant modified

574   vaccinia virus Ankara. Expert Rev Vaccines 2009;8(4):447-454.

575   14. Lambe T. Novel viral vectored vaccines for the prevention of influenza. Mol Med

576   2012;18:1153-1160.

577   15. Ledgerwood JE, DeZure AD, Stanley DA, Novik L, Enama ME, Berkowitz NM, Hu Z, Joshi G,

578   Ploquin A, Sitar S, Gordon IJ, Plummer SA, Holman LA, Hendel CS, Yamshchikov G, Roman F,

579   Nicosia A, Colloca S, Cortese R, Bailer RT, Schwartz RM, Roederer M, Mascola JR, Koup RA,

580   Sullivan NJ, Graham BS, the VRC 2007 Study Team. Chimpanzee Adenovirus Vector Ebola

581   Vaccine.   N Engl J Med 2017;376(10):928-938.

582   16. Ewer K, Rampling T, Venkatraman N, Bowyer G, Wright D, Lambe T, Imoukhuede EB, Payne

583   R, Fehling SK, Strecker T, Biedenkopf N, Krahling V, Tully CM, Edwards NJ, Bentley EM,

584   Samuel D, Labbe G, Jin J, Gibani M, Minhinnick A, Wilkie M, Poulton I, Lella N, Roberts R,

585   Hartnell F, Bliss C, Sierra-Davidson K, Powlson J, Berrie E, Tedder R, Roman F, De Ryck I,

586   Nicosia A, Sullivan NJ, Stanley DA, Mbaya OT, Ledgerwood JE, Schwartz RM, Siani L, Colloca

587   S, Folgori A, Di Marco S, Cortese R, Wright E, Becker S, Graham BS, Koup RA, Levine MM,

588   Volkmann A, Chaplin P, Pollard AJ, Draper SJ, Ballou WR, Lawrie A, Gilbert SC, Hill AV. A

589   Monovalent Chimpanzee Adenovirus Ebola Vaccine Boosted with MVA. N Engl J Med

590   2016;374(17):1635-1646.

591   17. Renteria SS, Clemens CC, Croyle MA. Development of a nasal adenovirus-based vaccine:

592   Effect of concentration and formulation on adenovirus stability and infectious titer during

593   actuation from two delivery devices. Vaccine 2010;28(9):2137-2148.

594   18. Evans RK, Nawrocki DK, Isopi LA, Williams DM, Casimiro DR, Chin S, Chen M, Zhu DM, Shiver

595   JW, Volkin DB. Development of stable liquid formulations for adenovirus-based vaccines. J

596   Pharm Sci 2004;93(10):2458-2475.

597   19. Kupgan G, Choudhari SP, Flynn NH, Nigatu A, Vupputuri S, Picking WL, Picking WD, Ramsey

598   JD Identification of Excipients for Stabilizing Fiberless Adenovirus as Biopharmaceuticals. J

599   Pharm Sci 2017;106(7):1764-1771.

600   20. Chen S, Guo D, Guo B, Liu J, Shen Y, Xu X, Huang W, Guo S. Investigation on formulation and

601   preparation of adenovirus encoding human endostatin lyophilized powders. International

602   journal of pharmaceutics 2012;427(2):145-152.

603   21. Stewart M, Ward SJ, Drew J. Use of adenovirus as a model system to illustrate a simple

604   method using standard equipment and inexpensive excipients to remove live virus

605   dependence on the cold-chain. Vaccine 2014;32(24):2931-2938.

606   22. LeClair DA, Cranston ED, Xing Z, Thompson MR. Evaluation of excipients for enhanced

607   thermal stabilization of a human type 5 adenoviral vector through spray drying. Int J Pharm

608   2016;506(1-2):289-301.

609   23. Jin TH, Tsao E, Goudsmit J, Dheenadhayalan V, Sadoff J. Stabilizing formulations for inhalable

610   powders of an adenovirus 35-vectored tuberculosis (TB) vaccine (AERAS-402). Vaccine
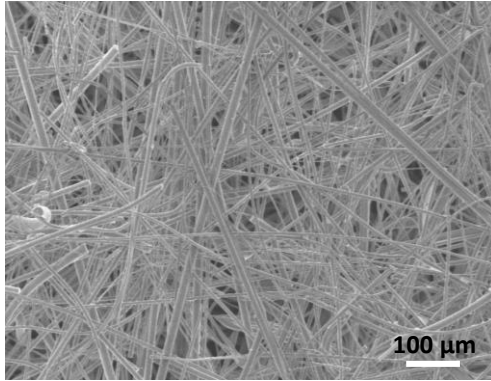
611   2010;28(27):4369-4375.

612   24. Afkhami S, LeClair DA, Haddadi S, Lai R, Toniolo SP, Ertl HC, Cranston ED, Thompson MR, Xing

613   Z. Spray dried human and chimpanzee adenoviral-vectored vaccines are thermally stable and

614   immunogenic in vivo. Vaccine 2017;35(22):2916-2924.

615   25. Pearson FE, McNeilly CL, Crichton ML, Primiero CA, Yukiko SR, Fernando GJ, Chen X, Gilbert

616   SC, Hill AV, Kendall MA. Dry-coated live viral vector vaccines delivered by nanopatch

617   microprojections retain long-term thermostability and induce transgene-specific T cell

618   responses in mice. PLOS ONE 2013;8(7):e67888.

619   26. Alcock R, Cottingham MG, Rollier CS, Furze J, De Costa SD, Hanlon M, Spencer AJ, Honeycutt

620   JD, Wyllie DH, Gilbert SC, Bregu M, Hill AVS. Long-Term Thermostabilization of Live Poxviral

621   and Adenoviral Vaccine Vectors at Supraphysiological Temperatures in Carbohydrate Glass.

622   Science Transl Med 2010; 2(19):19ra12-19ra12.

623   27. Dulal P, Wright D, Ashfield R, Hill AV, Charleston B, Warimwe GM. Potency of a

624   thermostabilised chimpanzee adenovirus Rift Valley Fever vaccine in cattle. Vaccine

625   2016;34(20):2296-2298.

626   28. Wang C, Dulal P, Zhou X, Xiang Z, Goharriz H, Banyard A, Green N, Brunner L, Ventura R,

627   Collin N, Draper SJ, Hill AVS, Ashfield R, Fooks AR, Ertl HC, Douglas AD. A simian-adenovirus-

628   vectored rabies vaccine suitable for thermostabilisation and clinical development for low-

629   cost single-dose pre-exposure prophylaxis. PLOS Negl Trop Dis 2018;12(10):e0006870-

630   e0006870.

631   29. O'Hara GA, Duncan CJA, Ewer KJ, Collins KA, Elias SC, Halstead FD, Goodman AL, Edwards NJ,

632   Reyes-Sandoval A, Bird P, Rowland R, Sheehy SH, Poulton ID, Hutchings C, Todryk S, Andrews

633   L, Folgori A, Berrie E, Moyle S, Nicosia A, Colloca S, Cortese R, Siani L, Lawrie AM, Gilbert SC,

634   Hill AVS. Clinical assessment of a recombinant simian adenovirus ChAd63: a potent new

635   vaccine vector. J Infect Dis 2012;205(5):772-781.

636   30. Dicks MD, Spencer AJ, Edwards NJ, Wadell G, Bojang K, Gilbert SC, Hill AV, Cottingham MG

637   2012. A novel chimpanzee adenovirus vector with low human seroprevalence: improved

638   systems for vector derivation and comparative immunogenicity. PlOS ONE

639   2012;7(7):e40385.

640   31. European Medicines Agency. Quality of medicines questions and answers: Part 2.

641   https://www.ema.europa.eu/en/human-regulatory/research-development/scientific-

642   guidelines/qa-quality/quality-medicines-questions-answers-part-2. Accessed November 27,

643   2019

644   32. Duddu SP, Dal Monte PR. Effect of Glass Transition Temperature on the Stability of

645   Lyophilized Formulations Containing a Chimeric Therapeutic Monoclonal Antibody. Pharm

646   Res 1997;14(5):591-595.

647   33. Hodge IM. Enthalpy relaxation and recovery in amorphous materials. J Non-Cryst Solids

648   1994;169(3):211-266.

649   34. Mansur HS, Sadahira CM, Souza AN, Mansur AAP. FTIR spectroscopy characterization of poly

650   (vinyl alcohol) hydrogel with different hydrolysis degree and chemically crosslinked with

651   glutaraldehyde. Mater Sci Eng C 2008;28(4):539-548.

652   35. Krimm S, Liang CY, Sutherland GBBM. Infrared spectra of high polymers. V. Polyvinyl alcohol.

653   J Polym Sci 1956;22(101):227-247.

654   36. U.S. Food and Drug Administration. Inactive Ingredient Search for Approved Drug Products

655   2016. https://www.accessdata.fda.gov/scripts/cder/iig/index.cfm

656   37. Rawat S, Gupta P, Kumar A, Garg P, Suri CR, Sahoo DK. Molecular mechanism of poly(vinyl

657   alcohol) mediated prevention of aggregation and stabilization of insulin in nanoparticles.

658   Mol Pharm 2015;12(4):1018-1030.

659   38. Liao Y-H, Brown MB, Jones SA, Nazir T, Martin GP. The effects of polyvinyl alcohol on the in

660   vitro stability and delivery of spray-dried protein particles from surfactant-free HFA 134a-

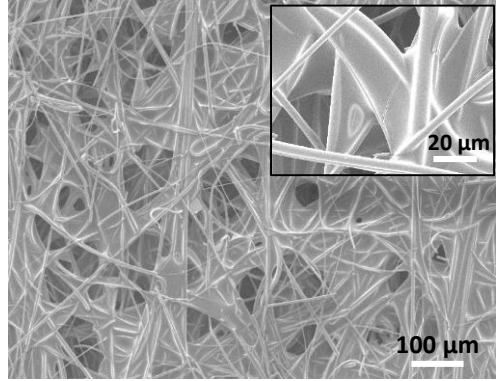661   based pressurised metered dose inhalers. Int J Pharm 2005;304(1–2):29-39.

662   39. Yoshioka S, Aso Y, Kojima S, Tanimoto T. Effect of polymer excipients on the enzyme activity

663   of lyophilized bilirubin oxidase and beta-galactosidase formulations. Chemical and

664   Pharmaceutical Bulletin 2000;48(2):283-285.

665   40. Sah H. Stabilization of proteins against methylene chloride/water interface-induced

666   denaturation and aggregation. J Control Release 1999;58(2):143-151.

667   41. Lai MC, Hageman MJ, Schowen RL, Borchardt RT, Topp EM. Chemical stability of peptides in

668   polymers. 1. Effect of water on peptide deamidation in poly(vinyl alcohol) and poly(vinyl

669   pyrrolidone) matrixes. J Pharm Sci 1999;88(10):1073-1080.
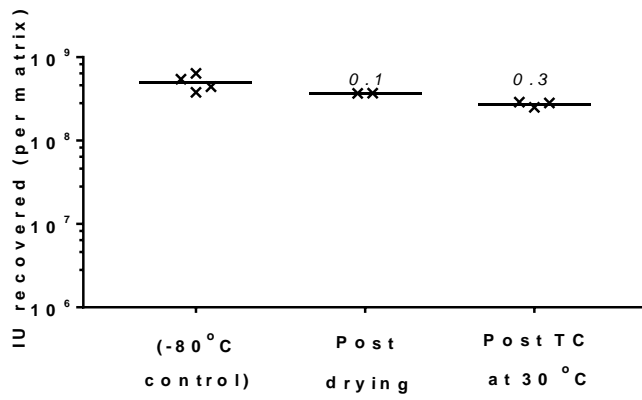
Figure 1
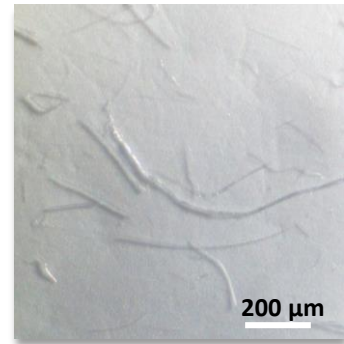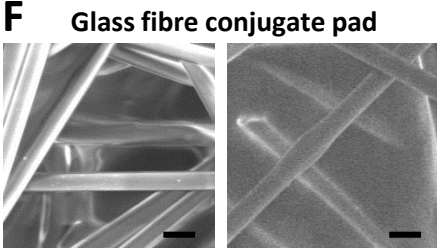
A

100 μm

B

20 μm

100 μm

C

IU recovered (per matrix)

10^9
10^8
10^7
10^6

(-80°C control)   Post drying   Post TC at 30°C

0.1   0.3

D

200 μm

Figure 2

A   Polypropylene J200

B   Polyester 23100

C   Polyamide 33100L

D   Cellulose 31ET CHR

E   Polyester leukosorb

F   Glass fibre conjugate pad

Figure 3

A

$r^2 = 0.27, p = 0.56$

Infectivity loss ($\log_{10}$-fold)

31ET CHR
Leu
23100
CP   J200
33100L
S14

Tg (^{o}C)

50   55   60

B

$r^2 = 0.70, 0.02$

Infectivity loss ($\log_{10}$-fold)

31ET CHR
Leu
23100   J200   CP
33100L
S14

Enthalpic recovery (J/g)

0   2   4   6   8

C

$r^2 = 0.35, p = 0.44$

Infectivity loss ($\log_{10}$-fold)

31ET CHR
Leu
23100
J200
33100L   CP
S14

Moisture content (% solid content)

4   6   8   10   12

D

$r^2 = 0.19, p = 0.32$

Infectivity loss ($\log_{10}$-fold)

31ET CHR
Leu
23100
33100L   CP
J200
S14

Protein loss ($\log_{10}$-fold)

-0.4   -0.2   0.0   0.2   0.4   0.6

Figure 4

A

B

Onset 220 °C

Normalized Heat Flow (w/g)

Temperature (°C)

C

Weight (%)

Deriv. Weight (% / °C)

262°C

553°C

Temperature (°C)

D

ATR units

PVA sample
PVA Mw 14K

1438

Wavenumber (cm⁻¹)

E

Hydrodynamic Diameter (nm)

Average MW (KDa)

F

S14
20
10
5
2
< 0.1

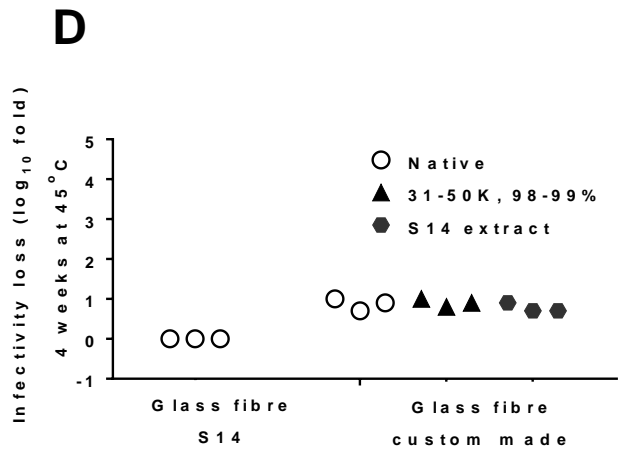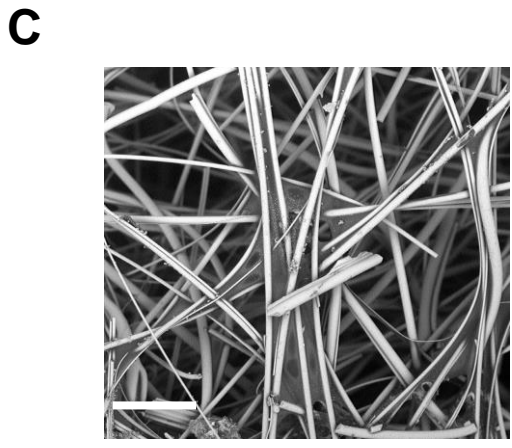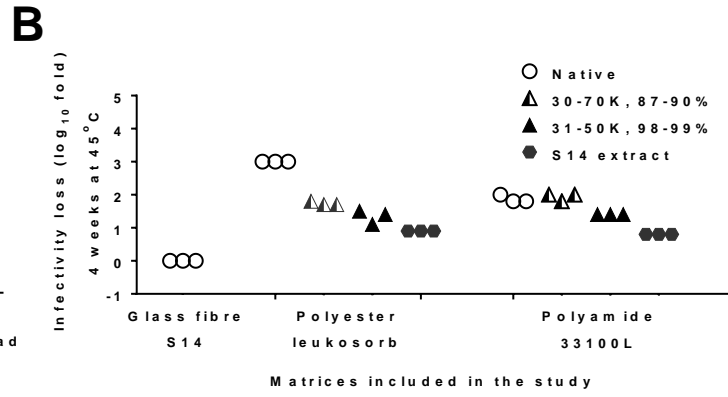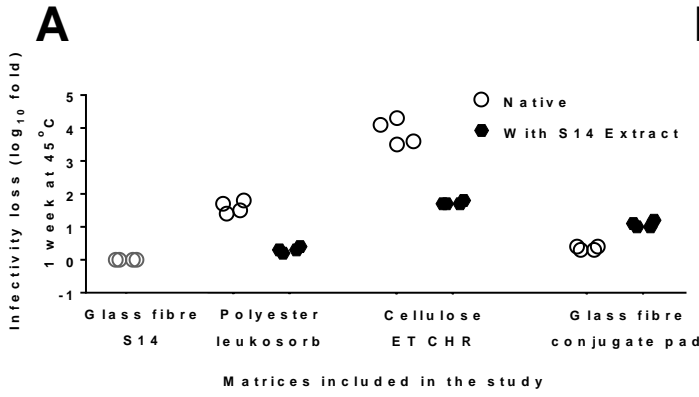4.0 3.5 3.0 2.5 2.0 1.5 ppm

Figure 5

Table 1: Basic characteristics of studied matrices

Matrix name (manufacturer product reference)	Manufacturer (sub-brand if applicable)	Main material	PS20 treatment?	Absorption >20 µL/cm² H₂O	Loading capacity (µL/cm²)	Fibre diameter (µm) ±SEM	Mean pore size (µm)	Thermostabilisation performance (log₁₀-fold infectivity loss)
S 14	GE (Whatman)	Glass fibre	X	✓	55	4.2±0.3	20	0.3
J200	Pall	Polypropylene	✓	✓	36	21.7±0.4	20	1
23100	Hollingsworth - Vose	Polyester	✓	✓	43	4.4±0.4	11	1.3
33100L	Hollingsworth - Vose	Polyamide	✓	✓	36	4.8±0.4	27	0.9
Cyclopore (PC)	GE (Whatman)	Polycarbonate	✓	X	Excl.	Excl.	Excl.	Excl.
31 ET CHR	GE (Whatman)	Cellulose	X	✓	40	15.4±1.0	1.2	2.4
Leukosorb (Leu)	Pall	Polyester[a]	X	✓	40	3.5±0.2	8	1.7
Conjugate pad (CP)	Pall	Glass fibre[b]	X	✓	30	12.3±0.4	N/A	0.9
Asymmetric polysulfone (AS)	Pall	Polysulfone	✓	X	Excl.	Excl.	Excl.	Excl.

Loading capacity was measured by weight measurement of matrices before and after full impregnation in water. Fibre diameter was measured using Image J from SEM micrograph images. Mean pore size are as provided in suppliers' specification (in one case N/A denotes data not available). Thermostabilisation performance presented is loss of infectivity after vaccine drying and thermochallenge for 1 week at 45 °C. Excl. denotes matrices excluded from further analysis on basis of loading capacity.

[a] Proprietary composition, but macroscopic, microscopic and FTIR spectrum appearances are consistent with polyester (data not shown); this matrix is henceforth referred to as polyester

[b] Henceforth referred to as 'glass fibre (conjugate pad)' for avoidance of confusion with S14.

Table 2: Physical characteristics of the glass fibre (S14) matrix

PARAMETER (unit)	Mean	Standard deviation
Area density [g.m^{-2}]	55.1	1.8
Thickness [mm]	0.5	0.04
Fibre diameter [μm]	3.4	1.8
Fibre length [mm]	4.4	1.5
Largest pore diameter [μm]	133.0	99.4
Mean flow pore diameter [μm]	22.3	0.5
Smallest pore diameter [μm]	6.4	1.5
Porosity [%]	95	
Capillary constant [cm^5]	7.7X10^{-7}	5.6X10^{-8}
Thermostabilisation buffer contact angle [^{o}]	30.9	4.9
Thermostabilisation buffer surface tension[(mN.m^{-1}]	63.9	0.3